Title

The three-dimensional architecture of chromatin in situ: electron tomography reveals fibers composed of a continuously variable zig-zag nucleosomal ribbon.

Journal

Journal of Cell Biology, 125(1)

ISSN

0021-9525

Authors

Horowitz, RA
Agard, DA
Sedat, JW
et al.

Publication Date

1994-04-01

DOI

10.1083/jcb.125.1.1

Peer reviewed

The Three-dimensional Architecture of Chromatin In Situ: Electron Tomography Reveals Fibers Composed of a Continuously Variable Zig-Zag Nucleosomal Ribbon

R. A. Horowitz, D. A. Agard,* J. W. Sedat,* and C. L. Woodcock

Department of Biology, University of Massachusetts, Amherst, Massachusetts 01003; and *Howard Hughes Medical Institute and Department of Biochemistry and Biophysics, University of California, San Francisco, California 94143

Abstract. The three dimensional (3D) structure of chromatin fibers in sections of nuclei has been determined using electron tomography. Low temperature embedding and nucleic acid–specific staining allowed individual nucleosomes to be clearly seen, and the tomographic data collection parameters provided a reconstruction resolution of 2.5 nm. Chromatin fibers have complex 3D trajectories, with smoothly bending regions interspersed with abrupt changes in direction, and U turns. Nucleosomes are located predominantly at the fiber periphery, and linker DNA tends to project toward the fiber interior. Within the fibers, a unifying structural motif is a two nucleosome-wide ribbon that is variably bent and twisted, and in which there is little face-to-face contact between nucleosomes. It is suggested that this asymmetric 3D zig-zag of nucleosomes and linker DNA represents a basic principle of chromatin folding that is determined by the properties of the nucleosome-linker unit. This concept of chromatin fiber architecture is contrasted with helical models in which specific nucleosome–nucleosome contacts play a major role in generating a symmetrical higher order structure. The transcriptional control implications of a more open and irregular chromatin structure are discussed.

THE beaded chain of nucleosomes that constitutes the basic structure of eukaryotic chromatin (van Holde, 1988) is folded and compacted to varying levels in vivo. The compaction state may be correlated with the transcriptional status of genomic segments (reviewed in Goldman, 1988) and there is strong evidence that the repression of large "domains" of chromatin is initiated and maintained through large-scale compaction (e.g., Kellum and Schedl, 1991). At present, our concept of chromatin organization within the living nucleus is limited by a lack of information about chromatin architecture.

A chromatin "30-nm" fiber is thought to represent a primary level of folding of the nucleosomal chain (van Holde, 1989), and considerable effort has been devoted to understanding the arrangement of nucleosomes and linker DNA within it (reviewed in Felsenfeld and McGhee, 1986; Widom, 1989). The great majority of this work has been carried out using chromatin that has been released from isolated nuclei following nuclease digestion and then examined in the electron microscope or by a variety of biochemical and biophysical techniques. Chromatin isolated in this way exhibits a 30-nm fiber morphology in solutions of appropriate ionic strength (e.g., Finch and Klug, 1976), and unfolds to a "beads-on-a-string" nucleosomal chain if the ionic strength is reduced below about 10-mM monovalent ions (e.g., Thoma et al., 1979). This reversible salt transition has been a primary target for studies of 30-nm fiber structure, and examination of unfolding intermediates led to the formalization of the "solenoid" model (Thoma et al., 1979) in which the linker DNA continues the superhelix established in the nucleosome. The solenoid model entails a 1-start helix of nucleosomes, with the linker DNA coiled between consecutive nucleosomes, and consecutive nucleosomes in the low salt beaded chain also consecutive in the fiber.

Other suggestions for the architecture of the 30-nm fiber have considered the "zig-zag" conformation of nucleosomes and linker DNA that is observable at intermediate ionic strengths to constitute the basic structural motif (e.g., Woodcock et al., 1984; Williams et al., 1986; Bordas et al., 1986). In these models, further compaction of the zig-zag leads to helical structures with quite different properties from the solenoid: the linker DNA is not coiled, but remains extended, and consecutive nucleosomes in the beaded chain are not consecutive in the 30-nm fiber. A common feature of all helical models that is well supported by biophysical measurements is the peripheral location and radial orientation of nucleosomes (Felsenfeld and McGhee, 1986). In addition to symmetrical, helical arrangements, a number of non-symmetrical proposals have been put forward, including

Address all correspondence to C. L. Woodcock, Department of Biology, University of Massachusetts, Amherst, MA 01003.

a supranucleosomal or "superbead" organization (e.g., Zentgraf and Franke, 1984) and a "layered" model (Subirana et al., 1985). To date, it has not been possible to prove that any of the model structures is correct. There are no methods for resolving linker DNA in isolated compact chromatin, and tomographic reconstructions have reported an asymmetric arrangement of nucleosomes (Woodcock et al., 1991*b*; Lawrence et al., 1989).

Recent evidence has shown that the process of chromatin isolation results in fibers that are altered from the in situ condition (Giannasca et al., 1993; Woodcock, 1994). Thus, it is more appropriate to study chromatin fibers in situ in the nucleus. Standard approaches to cellular ultrastructure involving epoxy resins and heavy metal stains are of limited value for the study of chromatin. Many of the procedures involved alter chromatin structures (Langmore and Paulson, 1983; Belmont et al., 1989), and the stains do not discriminate between nucleic acid and protein. However, low temperature methods have been shown to provide superior ultrastructural preservation (Armbruster et al., 1982; Carlemalm et al., 1982; Horowitz et al., 1990; Fullwood and Meek, 1993), and preferential DNA staining (Olins et al., 1989; Horowitz and Woodcock, 1992) allows resolution of nucleosomes and linker DNA in chromatin fibers (Woodcock et al., 1993).

In the present study, we have used low temperature preparation techniques and specific staining in combination with electron tomography to generate three-dimensional (3D)[1] reconstructions of chromatin fibers. The cell types used, starfish (*Patiria miniata*) sperm nuclei and chicken erythrocyte nuclei were selected for their clearly defined chromatin fibers, visible in situ in nuclei. Tomographic analysis of these specimens provides a resolution sufficient to image individual nucleosomes, and allows the complete 3D reconstruction of chromatin fibers without the prior assumption of internal symmetry.

We find that the chromatin fibers in these nuclei exhibit no long-range symmetry in the arrangement of nucleosomes and linker DNA. Rather, the fibers have a continuously variable structure, based on intricate folding and twisting of a 3D zig-zag of nucleosome-linker units. These findings are consistent with a chromatin architecture driven by the conformation of the nucleosome-linker unit (Woodcock et al., 1993), and generally incompatible with proposed helical models. A preliminary account of part of this work has appeared previously (Woodcock et al., 1992).

Materials and Methods

Specimen Preparation for Electron Microscopy

Chicken erythrocyte nuclei were isolated by the method of Ruiz-Carillo et al. (1980), then fixed in 3% glutaraldehyde (GA) in buffer containing 20 mM Na-cacodylate, pH 7.2, and 20 mM KCl at 4°C overnight. Sperm from the starfish *P. miniata* (Marinus Inc., Long Beach, CA) were released into artificial sea water, pH 8.0, on ice. Sperm heads and tails were separated with ten strokes in a Dounce homogenizer, and the nucleus-containing heads washed in 150 mM NaCl, 15 mM Hepes, pH 8.0, then fixed for 2 h in the same buffer containing 2% GA. Fixed chicken erythrocytes were rapidly frozen by spraying through an airbrush into liquid propane held at liquid nitrogen temperature, then dehydrated via freeze-substitution at −90°C in methanol prior to embedding in Lowicryl K11M, and UV polymerized at −55°C (Horowitz et al., 1990). Starfish sperm heads were dehydrated by progressively lowering the temperature and raising the concentration of methanol from 30% to 0°C to 97% at −55°C prior to UV polymerization in Lowicryl K11M at −55°C (Horowitz and Woodcock, 1992). Sections were cut at microtome (Reichert UltraCut E) settings between 90 and 120 nm, and stained either with uranyl and lead salts (Horowitz et al., 1990) or with the nucleic acid-specific osmium ammine-B stain (Olins et al., 1989) as described (Horowitz and Woodcock, 1992). After staining, sections were stabilized with a layer of evaporated carbon, and 5-nm colloidal gold particles adsorbed to the surface.

Data Collection and Tomographic Reconstruction

For electron tomography, the sections were observed in a Philips EM 430 at 150 kV, and, after pre-irradiation to allow beam-induced changes to occur, images were recorded at tilt intervals of 1.5° or 2.5° from −70° to +70° using a cooled CCD camera. The final pixel size was 1.25 nm. Alignment of the tilt series using gold bead positions, and reconstruction using weighted back projection was as described (Belmont et al., 1987) for six data sets of starfish sperm, and three data sets of chicken erythrocyte nuclei. Alignment accuracy was checked visually by viewing the tilt series as a "movie" loop; in addition, the alignment program provides a numerical value for the mean square difference between the expected and observed gold bead positions. This value never exceeded 10^{-3}, showing that the sections were accurately aligned and that beam-induced changes in the plane of the section during data collection were negligible. Normalization of the input images using areas of section devoid of material (Belmont et al., 1987) was not possible for many of the tilt series since at high tilts virtually all background regions became overlapped with chromatin. In these cases, normalization was based on the relative section thickness traversed by the electron beam at each tilt angle. Experimentation with a variety of normalization strategies showed that the normalization method had little influence on the final reconstructions.

We define the coordinate axes (x, y, and z) of the reconstructed volumes as follows: x and y are parallel to the plane of the untilted section with y parallel to the tilt axis; the z axis is perpendicular to the plane of the untilted section. The limiting resolution, d, for x-y planes of a reconstruction, is given by

$$d = (\pi * D)/N$$

where D is the diameter of a cylindrical object reconstructed from N equally spaced projections between ±90° (Crowther et al., 1970). For other objects, d varies according to the orientation and disposition of material within a section; for a 30-nm chromatin fiber running parallel to the tilt axis and not overlapped with other material, D may be considered as the width of the fiber. In this case, the final resolution (in the x-y plane) in these reconstructions is limited by the 1.25-nm sampling interval to 2.5 nm. For the "worst case" situation of densely packed material throughout a section of thickness (t), D is taken as the maximum specimen distance traveled by the electron beam:

$$t/\cos(\text{maximum tilt angle})$$

(Woodcock, 1992). This results in a resolution (in the x-y plane) of 6.4 nm, sufficient to resolve nucleosomes. Resolution in the z direction is estimated to be 1.5 to 2.0 times lower for reconstructions limited to ±60° of tilt (Carazo, 1992); considerable improvement in z resolution is reported when the data include higher tilt angles, such as the ±70° data used here (Baumeister et al., 1986).

Volume Visualization and Analysis

Reconstructed volumes were examined using VoxelView 3D volume rendering software (Vital Images Inc., Fairfield, IA). Understanding the complex structures required studying individual slices extracted from both orthogonal and non-orthogonal planes of the reconstructions, and interactive manipulation of complete or subset volumes. The 3D renderings were adjusted to high transparency for viewing through full volumes and densely packed regions. Embedded geometry displays of fiber trajectories were generated through interactive tracing of fiber axes in such volumes. Examination of shapes and quantitation of volumes of individual stain deposits was accomplished through selection of a "seed" voxel for 3D thresholding from raw voxel values. Linear distance measurements were derived from the 3D locations of points selected interactively, then refined by examination of lo-

1. *Abbreviations used in this paper*: GA, glutaraldehyde; 3D, three dimensional; 2D, two dimensional.

cal voxel value gradients; feature boundaries were defined by sharp drop-offs in the gradient.

Low Temperature, Low Dose Electron Microscopy

Sections of Lowicryl K11M embedded, osmium ammine B stained starfish sperm were examined at 100 kV in a Philips CM10 after cooling to −176°C in a cryoholder (Gatan Inc., Warrandale, PA), and tilt pairs (angular separation 25°) recorded under low dose (~15e^-/A^2) conditions, and subsequently with a dose equivalent to that used for tomography (~1.7E04e^-/A^2). Changes in fiber trajectory and overall section thickness with respect to temperature and dose were evaluated using the Sterecon system (Marko et al., 1988). The results reported here are part of a more extensive treatment of the topic to be described in detail elsewhere.

Modeling of Fiber Geometry

Computationally constructed fibers, modelled as described (Woodcock et al., 1993), were compared to the fibers in the reconstructions.

Results

Chromatin fibers were examined in situ to avoid the structural transitions involved in chromatin isolation (Giannasca et al., 1993). The starfish sperm preparations were stained with the nucleic acid–specific osmium ammine-B reagent (Olins et al., 1989; Horowitz and Woodcock, 1992) which provided a confident basis for interpretation of staining patterns. For comparison, data from chromatin fibers in chicken erythrocyte nuclei (stained with the less informative uranyl acetate/lead citrate combination) will also be discussed.

Starfish Sperm Chromatin

P. miniata sperm offer a number of advantages for studying chromatin fiber structure. Their nuclear proteins consist principally of a set of core histones similar to those of somatic cells, and a single major histone H1. Moreover, chromatin fibers are clearly seen in the nuclei when live sperm are fixed in seawater (Giannasca et al., 1993). Fixation of sperm heads in 150 mM NaCl, 15 mM Hepes, pH 8.0, after separation of heads and tails permits some expansion of the tightly packed nucleus (Fig. 1) with no change in fiber diameter relative to sea water fixed whole sperm, and none of the structural changes that accompany chromatin isolation (Giannasca et al., 1993). Viewed in projection, only short lengths of fiber appear continuous, and it is not apparent where changes in stain density might be related to overlap of structures. A section containing distinctly separated fibers is shown in stereo in Fig. 2. The fibers have highly variable paths, often containing sharp turns and folds, (*asterisks*) entering and exiting the plane of the section (*arrowheads*). The staining pattern represents deposition on and around nucleosomes, with fine, filamentous interconnections (e.g., Fig. 2, *bracketed region*).

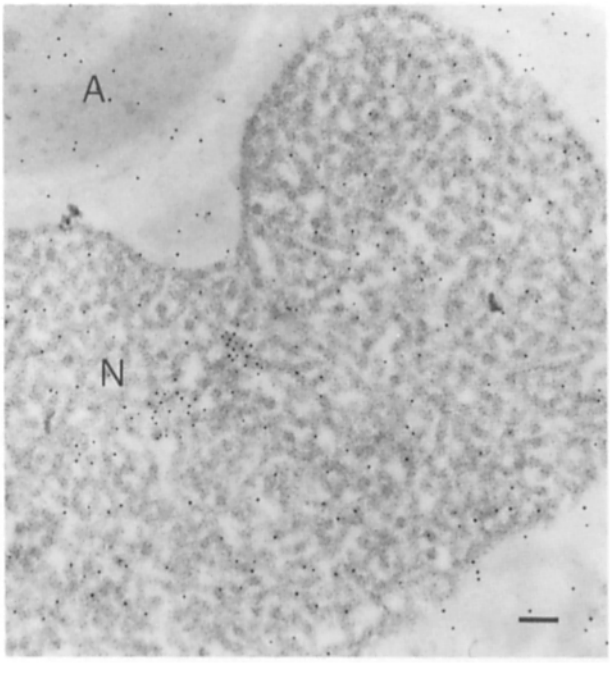

Figure 1. Section of starfish sperm prepared for tomography. The cup-shaped nucleus (*N*) contains chromatin fibers that are the only components contrasted with the osmium ammine-B reagent. At top left is the acrosome (*A*). Black dots are colloidal gold particles applied to the section surface for fiduciary marks. Nominal section thickness is 100 nm. Bar, 100 nm.

Electron Tomography: Data Collection and Reconstruction

Electron tomography and R-weighted back projection was used to obtain complete 3D reconstructions of sections of nuclei. With an accelerating voltage of 150 kV, it is possible to collect useful data up to 70° of tilt, reducing the reconstruction uncertainties imposed by the "missing wedge" effect (e.g., Carazo, 1992). The small tilt angle increment resulted in a final resolution of 2.5 nm in favorably oriented material (see Materials and Methods).

Pre-irradiation of sections to be used for tomographic data collection (Belmont et al., 1987) effectively prevented beam-induced changes occurring during data collection; colloidal gold applied to the surface of the section as fiduciary markers varied <1% from their predicted positions in the data sets. However, this pre-irradiation step resulted in reconstructions with, on average, 50% of the nominal section thickness indicated by the microtome setting. Although new developments in automated cryo-tomography promise reconstructions at greatly reduced doses (Koster et al., 1993), for this study the effect of beam-induced thickness reduction on the specimen contained within the section was investigated by comparing stereo pairs of sections recorded under minimal damage conditions (Luther, 1992; see Materials and Methods for low dose, low temperature imaging conditions) with data from the same areas collected conventionally. An 8% reduction in section thickness occurred between the first low dose stereo pair recorded at −176°C and a second pair recorded after prolonged irradiation at the same temperature. Within that area, the trajectory of a chromatin fiber was also measured and found to decrease by 8% in the z direction. The same area was recorded again after allowing the specimen to reach ambient temperature, and then exposing the section to a beam intensity and duration equivalent to that sustained during tomographic data collection. The section thickness was now 56% of the low dose value, but the z extent of the chromatin fiber trajectory had decreased by only 17%. Visually, a slight change in the trajectory of the fiber was noticeable, but the overall distribution of stain remained the same, with no superposition of stain density as

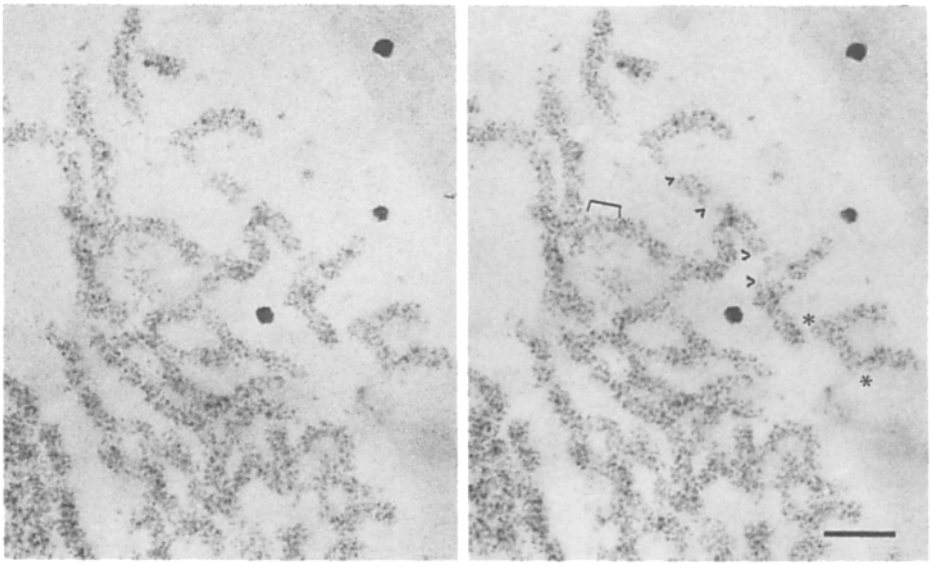

Figure 2. Stereo pair (angular separation 25°) of well-separated osmium ammine-B–stained starfish sperm chromatin fibers. The fine deposition of the stain on nucleosome-associated and linker DNA is evident in the bracketed region. Fibers enter and exit the plane of the section at locations marked by arrowheads. Note the sharp bends in a fiber trajectory at the asterisks. Nominal section thickness is 80 nm. Bar, 100 nm.

would be expected by a twofold compaction of the specimen itself. Rather, the impression was one of collapse of the plastic embedding medium around the specimen, which remained essentially unchanged.

In the reconstructions, mean 3D diameter measurements of fibers whose axes were primarily in the x–y plane were 31.5 nm, SD 1.3 nm, while those primarily in the z direction were 28.5 nm, SD 4.1 nm. The similarity of the values confirms that the chromatin fibers were not seriously compressed during beam-induced collapse of the embedding medium.

Chromatin Fibers Follow Complex 3D Trajectories

The 3D trajectories of a number of long, clearly defined fibers were determined by embedding an opaque tracing of the fiber axes within a transparently rendered volume (Fig. 3). The high transparency enables the full volume of the reconstruction to be viewed, but does not represent the original stain distribution. For example, a single slice of the area marked with the arrowhead in Fig. 3 is shown in Fig. 4 *d* with its original grey scale values. Fiber trajectories were continuously variable, ranging from smoothly sinuous regions to extremely abrupt changes and U turns, as suggested by single and stereo projection micrographs (Figs. 1 and 2). The mean 3D fiber diameter was 29.9 nm, SD 2.5 nm, similar to the 31.1 nm, SD 2.1 nm values obtained from two-dimensional (2D) projections of sectioned material (Giannasca et al., 1993).

In all of the reconstructions, there were regions where clearly defined fibers came together and could no longer be distinguished from one another. One example is indicated by the arrowhead in Fig. 3, a single slice of which is shown in Fig. 4 *d* (*arrow*). In most cases, the 3D appearance of these regions suggested some degree of interdigitation of fibers, rather than a simple side-to-side aggregation.

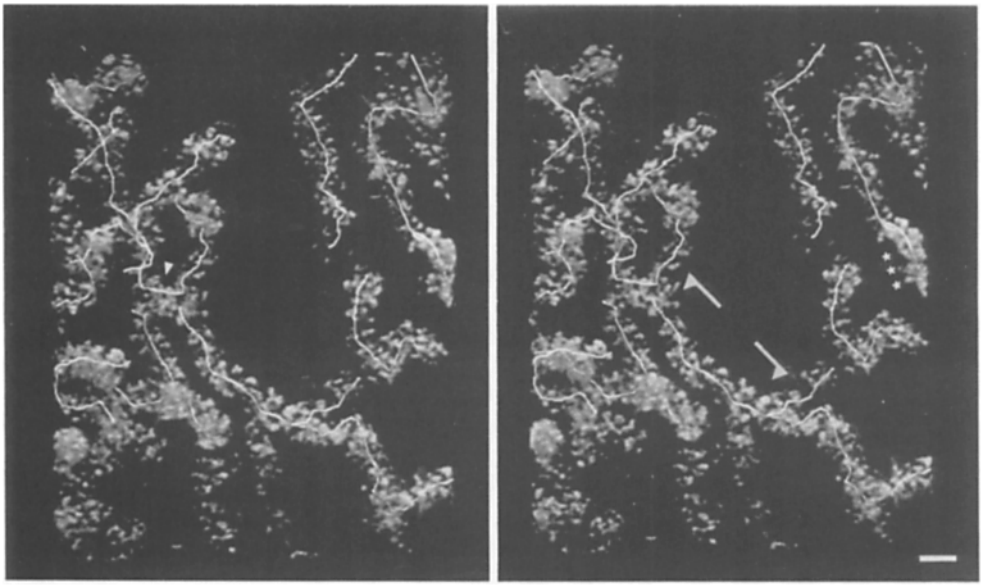

Figure 3. Stereo pair (angular separation 30°) of one of the six reconstructed volumes of starfish sperm heads. The volume has been rendered with maximum transparency to enable viewing through its entire thickness (60 nm). With these parameters, some voxels which contain densities related to the stain distribution are not visible in the final rendering. Some of the fiber axes have been marked. One area in which several fibers come together in such a way as to make their individual trajectories indistinguishable is denoted by the arrowhead. Bar, 100 nm.

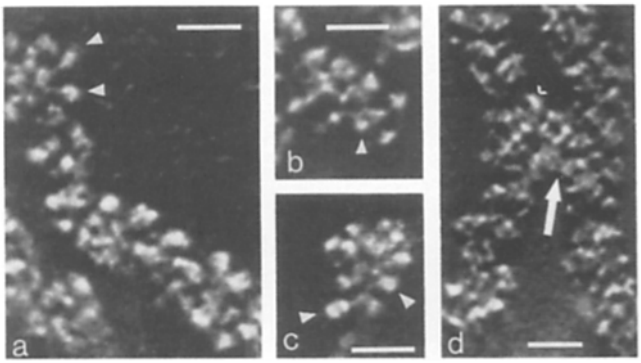

Figure 4. Single slices (x–y plane, thickness = 1.25 nm) from reconstructed volumes contain motifs resulting from different views of nucleosome-associated and linker DNA (*arrowheads*) within fibers. In *a* and *b*, a portion of the linker path between nucleosomes (*arrowheads*) can be followed within the plane of the single slice. Nucleosomes are identifiable in a region of interdigitated fibers (*d*; *arrow*); this is a single slice extracted from region denoted by the arrowhead in the volume shown in Fig. 3). Bars, 30 nm.

Figure 5. A subvolume containing a stain deposit of nucleosomal dimensions identified by selecting a "seed" voxel (see Materials and Methods). The area from which this seed was selected is denoted by the carat in Fig. 4 *d*. Successive views are rotated 15° on the y-axis. Bar, 10 nm.

Location of Nucleosomes within Fibers

Examination of both transparently rendered volumes (Fig. 3) and 1.25-nm thick slices of the reconstructed volumes (Fig. 4) reveals a detailed and interconnected distribution of stain within the chromatin fibers. The stain is preferentially deposited on DNA under the conditions used (Horowitz and Woodcock, 1992), and thus produces motifs resulting from different views of the nucleosome-linker unit. Fig. 3 and 4 contain numerous examples of nucleosome-shaped particles which have a mean diameter of 11.6 nm, SD 1.9 nm and thickness 6.5 nm, SD 1.3 nm. Fig. 5 shows the staining pattern expected from deposition on nucleosome-associated DNA; the mean dimensions of this region are 10.9 × 6.5 nm, with a volume of 345 nm^3 (200 bp of DNA has a volume of ~330 nm^3). The origin of this subvolume is denoted by the small arrowhead in Fig. 4 *d*, which contains an oblique segment of it.

Visual inspection of Figs. 3 and 4 shows that in many regions, nucleosome locations may be identified with confidence. They occur most frequently at the fiber periphery, are not spaced regularly along the fiber axis, and rarely contact one another. For the region of fiber denoted with brackets in Fig. 3, the mean nearest neighbor distance (center-to-center) for 16 nucleosomes is 13.9 nm, SD 2.3 nm. Another fiber in Fig. 3 with well-defined nucleosomes yielded a mean nearest neighbor distance of 11.2 nm, SD 1.8 nm. In these, and in most regions where individual fibers are clearly separated, nucleosomes are further apart from their neighbors than the ~6 nm expected for face-to-face contacts. In the regions, found in every reconstruction, where fibers are not clearly separated (e.g., Fig. 3, *arrowhead*), individual nucleosomes can still be recognized.

Individual nucleosomes often have a thin projection, presumed to be linker DNA. Examples can be seen in the volume representation in Fig. 3, and are marked by arrowheads in Fig. 4 (*a–c*), which show portions of the linker in single 1.25-nm thick slices (x–y plane) taken from that volume. The two linkers emanating from a nucleosome may be seen in Fig. 4 (*a* and *b*) (*arrowheads*). The mean 3D linker length of the examples in Fig. 4 was 17.3 nm, SD 2.4, equivalent to ~51 bp (the non-chromatosome linker of *P. miniata* is 56 bp, or ~19 nm). The linker DNA paths appear to traverse the fiber axis, rather than run parallel to it. This suggests that adjacent nucleosomes, along the fiber axis, are not consecutive ones along the DNA.

A Ribbon Motif Is Common

Within chromatin fibers no symmetrical positioning of nucleosomes was observed, although there are occasional short regions that show partial order. From a detailed examination of numerous regions of the reconstructions, aided by the interactive rotation of rendered volumes, we find that a common structural motif is a ribbon-like array of nucleosomes that is variably twisted and bent. Fig. 6 *a* contains a fiber displaying this motif in a sequence of 1.25-nm-thick slices (x–y plane) and a stereo pair of the transparently rendered volume containing those slices is shown in Fig. 6 *b*; Fig. 7 shows a stereo pair of a different volume rendered to illustrate the twisted, ribbon-like nature of the fiber.

Another example of the ribbon motif is seen in Fig. 8, illustrating a fiber that changes direction twice within a 28-nm-thick volume. Three consecutive 1.25-nm slices (x–y plane) from the top (Fig. 8 *a*), and bottom (*c*) portions show ribbon-like parallel arrays of nucleosomes, while in three consecutive slices from the center (*b*), the circular profile expected of a cylindrical fiber sectioned transversely is present. Stereo views of the complete volume, from above (Fig. 8 *d*) and below (*e*), illustrate the complex trajectory in this region. Examination of either view of the stereo pairs singly demonstrates that in projection, the complete volume gives little indication of the actual 3D organization.

A region in Fig. 3 denoted by three asterisks shows a highly twisted, ribbon-like fiber running nearly perpendicular to the plane of the section. The ribbon motif is also suggested by several fibers in Fig. 2.

Tomographic Reconstruction of Chicken Erythrocyte Nuclei

Erythrocyte data were collected from sections stained with uranyl and lead salts, and thus lacked the nucleic acid discrimination of the starfish material (Horowitz and Woodcock, 1992), making interpretation more difficult. The chicken erythrocyte chromatin fibers resembled those of the starfish sperm in having peripherally located nucleosomes, and no consistent nucleosome–nucleosome contacts. Ribbon-like arrays of diametrically apposed nucleosomes could be followed for short distances (Fig. 9). In general, fiber

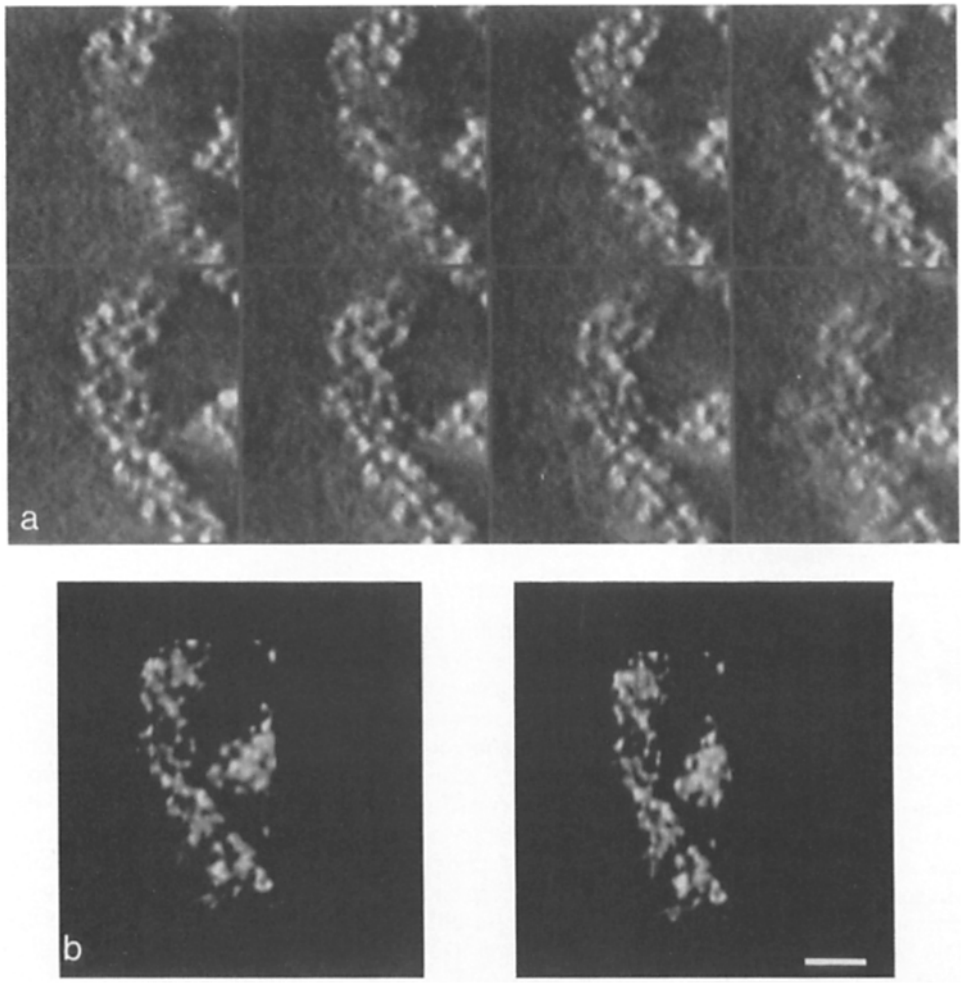

Figure 6. The twisted ribbon arrangement of a chromatin fiber is suggested by the distribution of stain in sequential 1.25-nm-thick x–y plane slices (*a*, *top left* to *bottom right*). The single slices are displayed with the "raw" reconstruction pixel values. The volume containing these slices, rendered for maximum transparency, was projected at ± 15° on the y axis to generate a stereo view (*b*). Bar, 30 nm.

trajectories in the erythrocyte nuclei were more complex than those in the starfish, and in a large proportion of the reconstructed volumes, fibers frequently appeared to be interdigitated with one another, seriously hampering the analysis of fiber architecture. The mean fiber diameter derived from the 3D data was 30.5 nm SD 2.1 nm, confirming the similarity of values between chicken erythrocyte and starfish sperm previously measured in single projections (Horowitz et al., 1990; Horowitz and Woodcock, 1992).

Discussion

We have used electron tomography to examine the 3D structure of chromatin in situ in a nucleus, starfish sperm, that

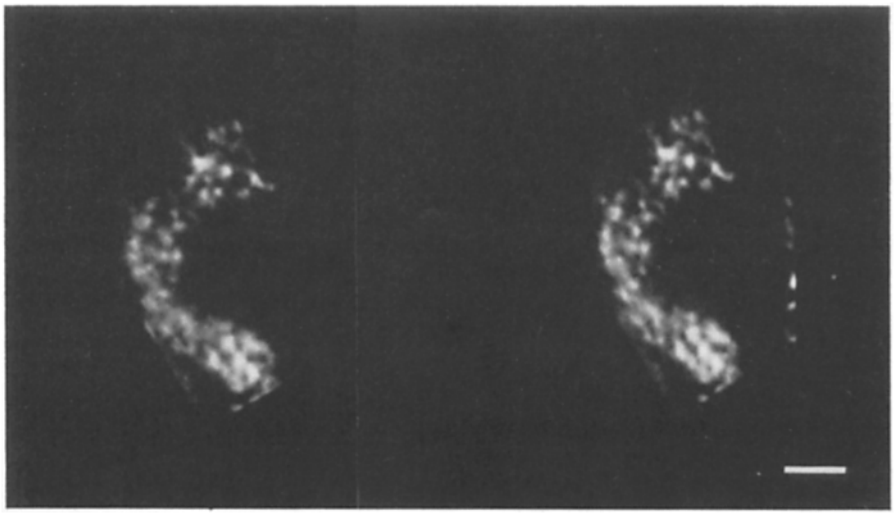

Figure 7. Stereo view (angular separation 30°) of a transparently rendered volume containing a fiber with a ribbon-like arrangement of nucleosomes; there is a pronounced twist in the central region. Bar, 30 nm.

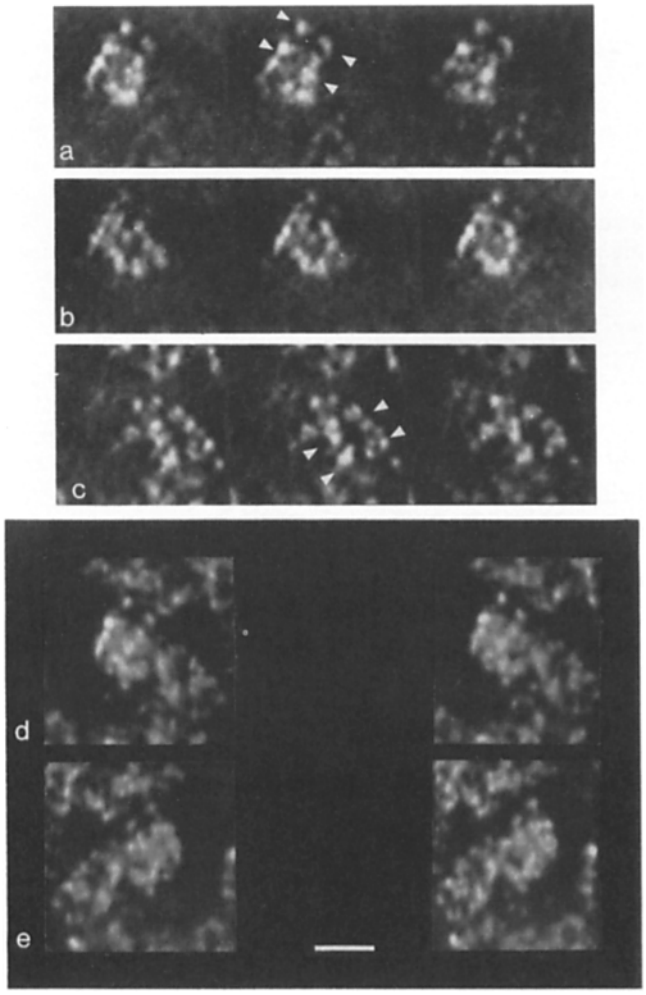

Figure 8. Example of the ribbon motif in a fiber that changes direction twice within a 28-nm-thick volume. Three consecutive 1.25-nm-thick x–y plane slices from the top (*a*), and bottom (*c*) portions of the volume show ribbon-like parallel arrays of nucleosomes (*arrowheads*). The central slices (*b*) suggest transverse sections of a cylindrical fiber. The transparently rendered volume, when viewed in stereo from the top (*d*) or the bottom (*e*), illustrates the complexity of this fiber's trajectory. Viewing either the left or right panel of *d* or *e* as a single 2D projection gives little indication of the 3D organization. Bar, 30 nm.

has extremely well-defined fibers (Fig. 1). Since the stain used has a strong preference for nucleic acids (and the starfish sperm nuclei contain little or no RNA) we have interpreted the stain distribution in terms of the location of nucleosomal and linker DNA. Moreover, the combination of intermediate voltage EM, direct digital acquisition with a CCD detector, high tilt angles, and small tilt increments provides reconstructions in which nucleosomes can be resolved with confidence.

The 30 nm Fiber as a Continuously Variable Structure

The reconstructions show no single, symmetrical arrangement of nucleosomes within the fibers, but rather a continuum of structures based on a ribbon-like arrangement of nucleosomes (Figs. 5–8). We suggest that the ribbon motif

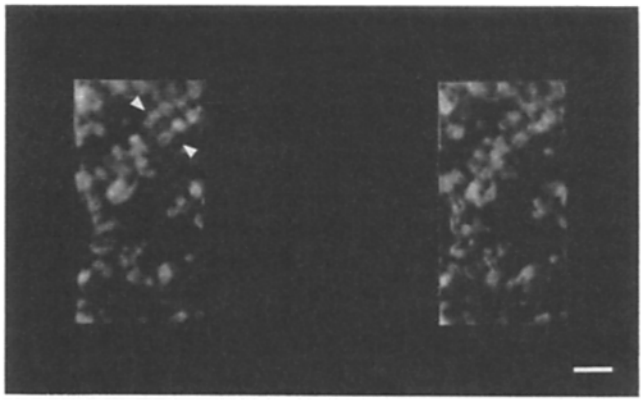

Figure 9. Detail from a 3D reconstruction of chromatin fibers in an isolated chicken erythrocyte nucleus, without DNA specific staining. A short ribbon-like array of diametrically apposed nucleosomes is present (*arrowheads*). Bar, 30 nm.

is the in situ homologue of the zig-zag ribbon conformation adopted by isolated chromatin under low salt conditions (Rattner and Hamkalo, 1978; Thoma et al., 1979; Woodcock et al., 1993). In isolated material, forced into a 2D conformation by adsorption to a support film, the ribbon is seen as two parallel lines of nucleosomes with linker DNA running between them in zig-zag fashion. In the 3D reconstructions, the ribbon conformation is seen as two lines of nucleosomes (Figs. 5–7, and 8, *a* and *c*). Linker DNA, when visible, traverses the fiber rather than runs parallel to it, as seen in Fig. 2 (*brackets*), Fig. 3, and Fig. 4 (*arrowheads*). The ribbon conformation is most easily recognized when it is flat (Fig. 8, *a* and *c*), or slightly twisted, as in Figs. 6 and 7. As the amount of twist increases, the cylindrical cross-section typical of many of the fibers in Fig. 3 is obtained, and the ribbon arrangement becomes less apparent.

Asymmetry in Fiber Structure Is Unlikely to be Preparation Induced

Symmetrical arrangements of nucleosomes promoted and maintained by mutual interactions have been a common feature of many earlier proposals for chromatin fiber structure (Felsenfeld and McGhee, 1986; Widom, 1989). In the expectation that a fiber built of identical subunits will indeed show symmetry, its absence in micrographs and reconstructions has sometimes been ascribed to a failure to preserve the native structure (e.g. Woodcock et al., 1991*b*). While the possibility that we are working with structures that have been degraded by the processes required for their observation can never be completely eliminated, we suggest that it is unlikely in this case. X-ray diffraction has demonstrated that the types of dramatic alteration caused by dehydration and embedding in epoxy (Langmore and Schutt, 1980) are mitigated when these procedures are carried out at low temperatures, using hydrophilic embedding media (Carlemalm et al., 1982). Low temperature embedding in Lowicryl K11M is also free of the specimen shrinkage that accompanies other embedding regimes (Fullwood and Meek, 1993). The substantial improvements in ultrastructural preservation available at low temperature in hydrophilic resins are also indicated by the excellent retention of antigenicity (e.g., Armbruster et al.,

1983), and evidence that the specificity of DNA staining with osmium ammine-B is based on the retention of specimen charge groups (Derenzini and Farabegoli, 1990). We have documented in considerable detail the improvement in ultrastructural preservation of chromatin and nuclei using these methods (Horowitz et al., 1990; Woodcock and Horowitz, 1992). Moreover, we have recently been able to examine frozen hydrated sections of starfish sperm nuclei. In these native specimens, the chromatin fibers are similar in diameter and appearance to those shown here, and show no changes in structure following nuclear swelling or glutaraldehyde fixation (Woodcock, 1994).

A separate issue pertinent to expectations of fiber symmetry is that chromatin does not, in fact, consist of identical subunits. Apart from the 146 bp of core particle DNA, all the components show considerable native inhomogeneity (van Holde, 1988). Of these, the variation in linker DNA length between consecutive nucleosomes (Lohr and van Holde, 1979; Strauss and Prunnell, 1982) is likely to dominate in making a symmetrical chromatin fiber energetically unfavorable (Athey et al., 1990; Widom, 1992).

Formation and Stability of Fibers Based on a 3D Zig-Zag

A fiber architecture based on a 3D zig-zag implies quite different mechanism(s) for formation and stability than proposed helical models. The latter demand specific interactions between nucleosomes to maintain helical symmetry, a feature that is clearly absent from the reconstructions. An alternative possibility that has been explored recently is that fiber formation is driven by the properties of the nucleosome-linker unit (Woodcock et al., 1993). Models based on the premise that the relative rotation between consecutive nucleosomes is dependent on the length of linker DNA, and taking into account the variation in linker DNA length between nucleosomes, generate "fibers" that exhibit a 3D zig-zag structure, and also show the types of variation in conformation and trajectory observed in the reconstructions. Fig. 10 *a* shows an example of a model chromatin "fiber" in which a constant linker DNA length and linker entry-exit angle create a symmetrical twisted ribbon-like structure (Woodcock et al., 1993). If the model calculation is repeated with a ±2-bp variation in linker DNA length and ±15° variation in linker entry–exit angle between nucleosomes, an asymmetrical "fiber" is obtained (Fig. 10 *b*). In some places, the ribbon-like arrangement is still apparent (*arrowheads*), but elsewhere, the asymmetry obtained is similar to the type observed in the reconstructions. Despite the dramatic loss of symmetry, the "fiber" structure is retained, as is the basic 3D zig-zag architecture, and the peripheral location of nucleosomes.

Linker DNA Conformation

A chromatin fiber structure based on a 3D zig-zag arrangement of nucleosomes and linker DNA retains the extended linker observed in isolated material at low ionic strengths. This type of linker conformation is a feature of two of the helical models proposed for chromatin architecture (Williams et al., 1986; Bordas et al., 1986). In contrast, in "solenoid" models of fiber architecture the linker DNA continues the superhelix defined by the nucleosome core (Felsenfeld and McGhee, 1986). We find no evidence for a uniformly curved linker in the reconstructions: on the contrary, when linker DNA (Fig. 4) is examined in 3D, it appears to traverse the fiber. This linker arrangement would place consecutive nucleosomes in non-adjacent positions. Additional support for an extended linker arrangement in vivo has come from studies of thymine dimer formation, which is favored in bent DNA, and occurs more frequently in nucleosomal than linker DNA (Pehrson, 1989; Pehrson and Cohen, 1992). Evidence for a salt-dependent (and H1-independent) bending of linker DNA exists for isolated dinucleosomes (Yao et al., 1990, 1991), but has yet to be demonstrated in polynucleosomes or in vivo.

Relation to Previous Studies of Fiber Architecture

Previous studies of chromatin architecture, using diverse techniques and starting material, have resulted in a variety of proposed structures (reviewed in Felsenfeld and McGhee, 1986; Widom, 1989). Comparisons between these studies, as well as with the present one, are complicated by this diversity. The issue of chromatin compaction under different ionic

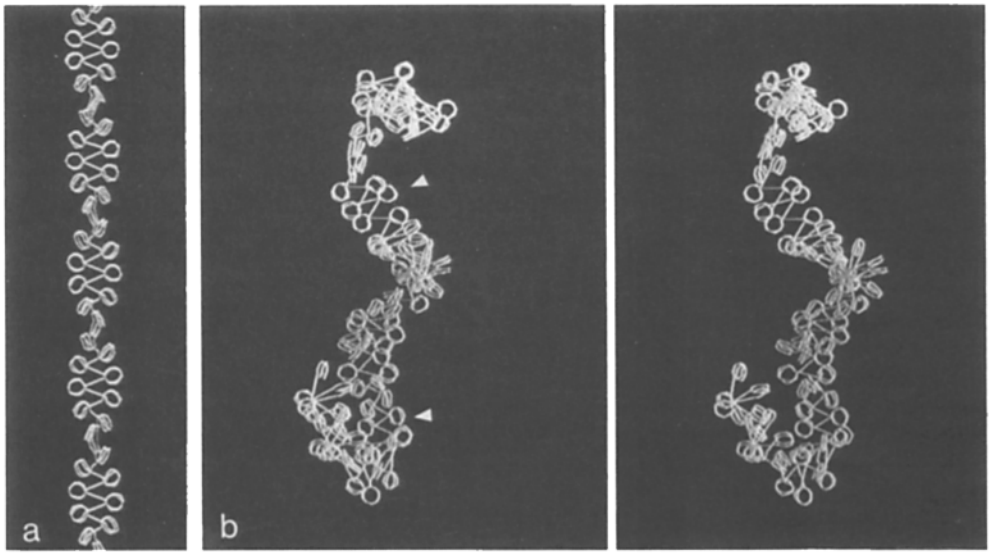

Figure 10. Models of chromatin fiber formation based on properties of the nucleosome-linker unit. Models based on fixed linker DNA length and entry–exit angle generate symmetrical "fibers" (*a*). Variations in linker length (±2 bp) and entry–exit angle (±15°) generate a twisted, folded "fiber" (*b*) similar to those seen in the reconstructions, with short regions (*arrowheads*) in which a symmetrical arrangement (as in *a*) is visible.

conditions provides a good example of the problem. Isolated chromatin fibers from many sources, including starfish sperm, are highly compact in buffers containing 150 mM monovalent ions, and tend to aggregate and precipitate (van Holde, 1988; Giannasca et al., 1993). In contrast, such media promote a mild separation of fibers in situ (Figs. 1 and 2), maintaining the open conformation seen throughout these reconstructions. This major difference in compaction response suggests that direct comparisons of compaction data derived from isolated chromatin in solution with fibers in situ should be avoided. Similar difficulties arise in comparisons of other chromatin properties.

The closest opportunity for comparison of in situ, 3D structural information at the fiber level is a tomographic reconstruction of intact chromatin fibers in sections of hypotonically shocked echinoderm (*Holothuria tubulosa*) sperm nuclei (Subirana et al., 1985) which also featured an asymmetric arrangement of nucleosomes. However, the "layered" organization proposed in that study is not seen in the reconstructions presented here.

In general terms, the most striking differences between the proposed helical models of fiber structure and our tomographic data are the asymmetry of nucleosome positions, and the absence of face-to-face nucleosome contacts. Two obvious questions then arise. First, is isolated chromatin, from which the models have been derived, more "ordered" than in situ chromatin? Since all previous tomographic studies of isolated chromatin have found asymmetrical arrangements of nucleosomes (Subirana et al., 1985; Lawrence et al., 1989; Woodcock et al., 1991*b*), this appears unlikely. Second, has the mild dispersion of fibers used in this study resulted in the loss of face-to-face nucleosome contacts? Examination of nuclei that have been swollen to different degrees reveals no changes in fiber architecture, suggesting that all but subtle changes in inter-nucleosomal distances may be excluded.

The evident differences between in situ and isolated chromatin, and the paucity of in situ data make it important to focus more effort in the future on the intact chromatin conformations that are present in the nucleus.

Implications for Chromatin Function

An asymmetrical 3D zig-zag of nucleosomes would generally present a more open substrate to the transcriptional regulatory machinery than helical models with strong nucleosome–nucleosome contacts. Under these conditions, the concept of chromatin components "inside" the fiber and sequestered, versus "outside" and accessible, becomes a strictly "local" phenomenon, rather than a general property. Gene repression in compact chromatin may then be seen as an issue of accessibility related to the local architecture of a continuously variable chromatin fiber.

A related issue is the absence, in conventional electron micrographs, of well-defined chromatin fibers in all but a few specialized nuclei, including the avian and echinoderm nuclei investigated here. In mapping fiber trajectories and nucleosome positions in the reconstructed volumes of either origin, we frequently encountered regions in which clearly separate fibers came together in such a way as to make their individual paths undefinable, and precluded the assignment of a given nucleosome position to one or another of the fibers. We suggest that in these regions, interdigitation of fibers is occurring. This may represent the type of fiber–fiber interaction which results in the condensed chromatin typically seen in eukaryotic nuclei. With a more open, asymmetrical organization and widespread interdigitation, it is possible to envisage a nucleus in which the chromatin retains the basic 3D zig-zag structure reported here, yet lacks canonical 30-nm fibers. Accessibility to regulatory molecules then becomes a property of the chromatin mass, rather than solely of fiber architecture.

The present study offers a novel, 3D, ultrastructural context for nuclear function. Furthermore, the ability to obtain high quality 3D information from minimally perturbed specimens stained to discriminate between protein and nucleic acid components provides a basis for addressing the state of chromatin in nuclei in general. Whether it is appropriate to continue to view chromatin organization in terms of the classical hierarchy of specific folding levels is an important goal of future tomographic studies.

Supported by National Science Foundation DCB 85-1388 and National Institutes of Health GM43786 to C. L. Woodcock, NIH GM 31267 to D. A. Agard, and NIH GM25101 to J. W. Sedat. The Microscopy and Imaging Facility (University of Massachusetts, Amherst, MA) is supported in part by NSF BBS 87-14235. We are grateful to M. Marko (Wadsworth Center, Albany, NY) for use of the STERECON system, supported in part by NIH Biotechnology Resource grant RR 01219.

Received for publication 20 September 1993 and in revised form 6 January 1994.

References

Armbruster, B. L., E. Carlemalm, R. Chiovetti, R. M. Garavito, J. A. Hobot, E. Kellenberger, and W. Villiger. 1982. Specimen preparation for electron microscopy using low temperature embedding resins. *J. Microsc.* 126: 77–85.

Athey, B. D., M. F. Smith, S. F. Williams, D. A. Rankert, and J. P. Langmore. 1990. The diameters of frozen hydrated Thyone and Necturus chromatin fibers increase with DNA linker length: evidence in support of variable diameter models for chromatin. *J. Cell Biol.* 111:785–806.

Baumeister, W., M. Barth, R. Hegerl, R. Guckenberger, M. Hahn, and W. O. Saxton. 1986. Three dimensional structure of the regular surface layer (HPI layer) of *Deinococcus radiourans*. *J. Mol. Biol.* 187:241–253.

Belmont, A. S., J. W. Sedat, and D. A. Agard. 1987. A three-dimensional approach to mitotic chromosome structure: evidence for a complex hierarchical organization. *J. Cell Biol.* 105:77–92.

Belmont, A. S., M. B. Braunfeld, J. W. Sedat, and D. A. Agard. 1989. Large-scale chromatin structural domains within mitotic and interphase chromosomes in vitro and in vivo. *Chromosoma.* 98:129–143.

Bordas, J., L. Perez-Grau, M. H. J. Koch, M. C. Vega, and C. Nave. 1986. The superstructure of chromatin and its condensation mechanism II: Theoretical analysis of the X-ray scattering patterns and model calculations. *Eur. Biophys. J.* 13:175–185.

Carazo, J.-M. 1992. The fidelity of 3D reconstructions from incomplete data and the use of restoration methods. *In* Electron Tomography. J. Frank, editor. Plenum Press, New York. 117–164.

Carlemalm, E., R. M. Garavito, and W. Villiger. 1982. Resin development for electron microscopy and an analysis of embedding at low temperature. *J. Microsc.* 126:123–143.

Crowther, R. A., D. J. DeRosier, and A. Klug. 1980. The reconstruction of a three dimensional structure from its projections, and its application to electron microscopy. *Proc. Roy. Soc. Lond. Ser. A.* 317:319–340.

Derenzini, M., and F. Farabegoli. 1990. Selective staining of nucleic acids by osmium-ammine complex in thin sections from Lowicryl-embedded samples. *J. Histochem. Cytochem.* 38:1495–1501.

Felsenfeld, G., and J. D. McGhee. 1986. Structure of the 30 nm chromatin fiber. *Cell.* 44:375–377.

Fullwood, N. J., and K. M. Meek. 1993. A synchrotron X-ray study of the changes occurring in the corneal stroma during processing for electron microscopy. *J. Microsc.* 169:53–60.

Giannasca, P. J., R. A. Horowitz, and C. L. Woodcock. 1993. Transitions between in situ and isolated chromatin. *J. Cell Sci.* 105:551–561.

Goldman, M. A. 1988. The chromatin domain as a unit of gene regulation. *Bioessays.* 9:50–55.

Horowitz, R. A., and C. L. Woodcock. 1992. Alternative staining methods for Lowicryl sections. *J. Histochem. Cytochem.* 40:123–133.

Horowitz, R. A., P. J. Giannasca, and C. L. Woodcock. 1990. Ultrastructural preservation of nuclei and chromatin: improvement with low temperature methods. *J. Microsc. (Oxf.).* 157:205–224.

Kellum, R., and P. Schedl. 1991. A position assay for boundaries of higher order chromatin domains. *Cell.* 64:941–950.

Koster, A. J., M. B. Braunfeld, J. Fung, C. K. Abbey, K. F. Han, W. Liu, H. Chen, J. W. Sedat, and D. A. Agard. 1993. Towards automatic three-dimensional imaging of large biological structures using intermediate voltage electron microscopy. *Microsc. Soc. Am. Bull.* 23:176–188.

Langmore, J. P., and J. R. Paulson. 1983. Low angle X-ray diffraction studies of chromatin structure in vivo and in isolated nuclei and metaphase chromosomes. *J. Cell Biol.* 96:1120–1131.

Lawrence, M. C., M. A. Jaffer, and B. T. Sewell. 1989. The application of the maximum entropy method of electron microscopy tomography. *Ultramicroscopy.* 31:285–302.

Lohr, D., and K. E. van Holde. 1979. Organization of spacer DNA inc chromatin. *Proc. Natl. Acad. Sci. USA.* 76:6325–6330.

Luther, P. K. 1992. Sample shrinkage and radiation damage. *In* Electron Tomography. J. Frank, editor. Plenum Press, New York. 39–60.

Marko, M., D. Leith, and D. Parsons. 1988. Three-dimensional reconstruction of cells from serial sections and whole-cell mounts using multilevel contouring of stereo micrographs. *J. Electron. Microsc. Tech.* 9:395–411.

Olins, A. L., B. A. Moyer, S. Kim, and D. P. Allison. 1989. Synthesis of a more stable osmium ammine electron dense stain. *J. Histochem. Cytochem.* 37:395–398.

Pehrson, J. R. 1989. Thymine dimer formation as a probe of the path of DNA in and between nucleosomes in intact chromatin. *Proc. Natl. Acad. Sci. USA.* 86:9149–9153.

Pehrson, J. R., and L. H. Cohen. 1992. Effects of DNA looping on pyrimidine dimer formation. *Nucleic Acids Res.* 20:1321–1324.

Rattner, J. B., and B. A. Hamkalo. 1978. Higher order structure in metaphase chromosomes. *Chromosoma.* 69:363–379.

Strauss, F., and A. Prunell. 1983. Organization of interchromosomal DNA in rat liver chromatin. *EMBO (Eur. Mol. Biol. Organ.) J.* 2:51–56.

Subirana, J. A., S. Munoz-Guerra, J. Ayami, M. Radermacher, and J. Frank. 1985. The layered organization of nucleosomes in 30 nm chromatin fibers. *Chromosoma.* 91:377–390.

Thoma, F., T. Koller, and A. Klug. 1979. Involvement of histone H1 in the organization of chromatin and the salt-dependent superstructures of chromatin. *J. Cell Biol.* 83:403–427.

van Holde, K. E. 1988. Chromatin. Spinger Verlag, New York. 497 pp.

Widom, J. 1989. Toward a unified model of chromatin folding. *Annu. Rev. Biophys. Biophys. Chem.* 18:365–395.

Widom, J. 1992. A relationship between the helical twist of DNA and the ordered positioning of nucleosomes in all eukaryotic cells. *Proc. Natl. Acad. Sci. USA.* 89:1095–1099.

Williams, S. P., B. D. Athey, L. J. Muglia, R. S. Schappe, A. H. Gough, and J. P. Langmore. 1986. Chromatin fibers are left-handed helices with diameter and mass per unit length that depend on linker length. *Biophys. J.* 49:233–248.

Woodcock, C. L. 1992. The organization of chromatin and chromosomes. *In* Electron Tomography. J. Frank, editor. Plenum Press, New York. 313–357.

Woodcock, C. L. 1994. Chromatin fibers observed in situ in frozen hydrated sections. Native fiber diameter is not correlated with nucleosome repeat length. *J. Cell Biol.* 125:11–19.

Woodcock, C. L., L.-L. Y. Frado, and J. B. Rattner. 1984. The higher order structure of chromatin: evidence for a helical ribbon arrangement. *J. Cell Biol.* 99:42–52.

Woodcock, C. L., H. Woodcock, and R. A. Horowitz. 1991*a*. Ultrastructure of chromatin. I. Negative staining of isolated fibers. *J. Cell Sci.* 99:99–106.

Woodcock, C. L., B. F. McEwen, and J. Frank. 1991*b*. Ultrastructure of chromatin. II. Three-dimensional reconstruction of isolated fibers. *J. Cell Sci.* 99:107–114.

Woodcock, C. L., R. A. Horowitz, and D. A. Agard. 1992. Three-dimensional organization of chromatin fibers in situ examined by EM tomography. *In* Proc. 50th Annu. Mtg. Electron Microsc. Soc. Am. G. W. Bailey, J. Bently, and J. A. Small, editors. San Francisco Press, San Francisco, CA. 498–499.

Woodcock, C. L., S. A. Grigoryev, R. A. Horowitz, and N. Whitaker. 1993. A folding model for chromatin that incorporates linker DNA variability produces fibers that mimic the native structures. *Proc. Natl. Acad. Sci. USA.* 90:9021–9025.

Yao, J., P. T. Lowary, and J. Widom. 1990. Direct detection of linker bending in defined-length oligomers of chromatin. *Proc. Natl. Acad. Sci. USA.* 87:7603–7607.

Yao, J., P. T. Lowary, and J. Widom. 1991. Linker DNA bending induced by the core histones of chromatin. *Biochemistry.* 30:8408–8414.

Zentgraf, H., and W. W. Franke. 1984. Differences of supranucleosomal organization in different kinds of chromatin: cell-type specific globular subunits. *J. Cell Biol.* 99:272–286.